Available online at www.sciencedirect.com
ScienceDirect
Scripta Materialia 61 (2009) 1145–1148
Scripta MATERIALIA
www.elsevier.com/locate/scriptamat

# Complexity of shear localization in a Zr-based bulk metallic glass

J. Zhang,[a,b] P. Aimedieu,[a] F. Hild,[a] S. Roux[a,*] and T. Zhang[b]

[a] *LMT-Cachan, ENS Cachan/CNRS/UPMC/PRES UniverSud Paris, 61 Avenue du Président Wilson, F-94235 Cachan Cedex, France*
[b] *Department of Materials Science and Engineering, Beijing University of Aeronautics and Astronautics, Beijing 100191, China*

Received 23 May 2009; revised 20 August 2009; accepted 26 August 2009
Available online 1 September 2009

The compressive behaviour of a Zr-based metallic glass was studied in situ through optical and infrared imaging. Results show that localization bands are more complex than simple planes, and interactions between different slip systems are an essential ingredient to understanding slip arrest and hence the ultimate strain such materials sustain. Roughness, which is responsible for both the damage and arrest mechanisms, is argued to be another key feature that enhances the ultimate macroscopic shear strain.


*Keywords:* Metallic glass; Shear bands; Compression test; Digital image correlation

Metallic glasses have been the subject of numerous studies. After their discovery [1], they were considered as exotic materials that required such a quick quenching rate to preserve their amorphous structure that the processing conditions drastically limited their potential usage. A significant advance occurred when compositions and the copper mold casting method allowing for bulk material synthesis were found [2]. The amorphous structure of bulk metallic glasses (BMGs) prevents the occurrence of large defects such as dislocations. Plasticity is still possible because of local structural rearrangements, but the yield stress is much higher than that of the corresponding crystalline phases. This remarkable feature is very attractive and has motivated further research for high-performance applications. However, above the yield stress, the plastic flow of BMGs tends to localize into shear bands, and hence the onset of yielding may appear as leading to fast, brittle-like failure. Thus, in order to enhance the mechanical properties of BMGs, understanding and mastering this localization process would appear to be essential.

The highly localized heterogeneous deformation behaviour of the BMG samples is usually manifested by serrated plastic flow [3–6]. After yielding, plastic flow is observed by irregular and regular serrations that are characterized by sudden load/stress drops separated by elastic reloading. Different interpretations on the persistence or renewal of slip bands corresponding to the stress drops are still debated. The occurrence of multiple shear bands is already reported in the literature, but no convincing explanation was suggested as to why these shear bands, akin to brittle cracks, do not lead to failure as soon as they appear. How is it possible that the sample may sustain so many of these shear bands?

Experimental evidence was also published confirming an intense heat release along shear bands. This dissipation is extremely localized in space and time. The temperature rises observed by infrared (IR) thermography are small (about 1 K [8,10]) because of the time and space integration. Extrapolations to the source lead to very high temperature rises (more than a few hundred degrees kelvin), an interpretation supported by the observation of melting of a very thin tin coating close to shear bands [7]. Moreover, the fractured surface reveals river-like patterns that suggest that the extreme surface (the "heart" of the final localization band) has experienced a temperature level close to or above the glass transition temperature. However, although this high dissipation undoubtedly takes place, the issue of whether adiabatic localization is the primary mechanism for initiating (rather than the consequence of) macroscopic shear banding remains unclear. It is therefore important to carry out in situ observations of plastic deformation processes of BMGs using various characterization means [8–12].

For this work, $Zr_{62}Cu_{15.5}Ni_{12.5}Al_{10}$ BMG was chosen for its good glass-forming ability and outstanding plastic deformability [13]. Uniaxial compression tests with

* Corresponding author. Tel.: +33 1 47402834; fax: +33 1 47402240; e-mail: stephane.roux@lmt.ens-cachan.fr

1359-6462/$ - see front matter © 2009 Acta Materialia Inc. Published by Elsevier Ltd. All rights reserved.
doi:10.1016/j.scriptamat.2009.08.041

synchronized observation by both IR and digital cameras were carried out in order to investigate the deformation mechanism.

As-cast 2 mm diameter rods with an aspect ratio of 2:1 were carefully sliced by a diamond-tipped disc saw. The cross-section of each sample was polished to almost a mirror finish using 2000 grit paper. The amorphous structure of the as-cast samples was confirmed by X-ray diffraction. Test samples were ultrasonically cleaned in acetone, then one half of the cylindrical surfaces of the samples was coated with a thin layer of colloidal white paint onto which a black paint was sprayed to form a texture suited for digital image correlation (DIC), and the other half was coated with only a thin layer of carbon black coating in order to optimize emissivity for IR imaging.

Compression tests were carried out on a servohydraulic testing machine with a macroscopic strain rate of $1.25 \times 10^{-3}\ s^{-1}$. Digital and IR cameras were employed face to face along a direction perpendicular to the cylindrical axis for in situ observations. The resolution of the former is $1300 \times 1950$ pixels$^2$ and the dynamic range is 12 bits per colour. For DIC analyses, the pictures were converted to a greyscale image, and the magnification was set to 4.3 μm pixel$^{-1}$. An IR camera with both silicon and ZnSe lenses was used. This device detects IR radiations in the 3.6–5.1 μm wavelength range. The temperature resolution of the IR camera is less than 0.05 K, while the spatial resolution of the image is about 30 μm pixel$^{-1}$. This camera was used to capture $92 \times 208$ pixel$^2$ images at a rate of 100 frame s$^{-1}$. The surface morphology of deformed samples was characterized by scanning electron microscopy (SEM).

The apparent (macroscopic) stress–strain displays an elastic behaviour up to ca. 1.5 GPa, followed by an extended plastic plateau with numerous serrations and finally an apparent decrease in the flow stress just prior to failure. A local temperature rise occurs simultaneously with each stress drop, confirming that the shear bands are detected from the temperature history; the higher the stress drop, the larger the temperature increment, as could have been anticipated. It is thus possible to capture the shear band associated with each serration.

At those instants, the temperature maps shown in Figure 1 clearly show a hot trace appearing on the surface of the sample with an approximate elliptical shape corresponding to a slip along a maximum shear plane (at 45° with respect to the compression axis). In spite of the short inter-frame time, the spatial extent of these bands appears to be broad, essentially because of heat diffusion from the slip plane. Some pictures show remarkable features, namely, the temperature increment appears to be highly asymmetric, signalling non-uniform slip (Fig. 1, left). At other times, a kink is observed in the trace of the slip band, suggesting that the support of slip consists of at least two such planes crossing each other (Fig. 1, right). This reveals an unexpected complexity in the geometry of these slip events.

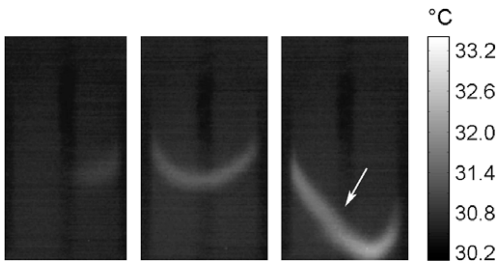


**Figure 1.** Three IR camera images after shear band slips during the experimental test. Note that the left image shows a partial slip or rotation, while the right one displays a kink (shown with an arrow) that can be interpreted as the mobilization of two slip planes.

It is also worth noting that at the initial stage of plasticity many slip events take place, with minute, barely detectable stress drops. The surface trace of these bands appears to be spread over a large region. As the total strain increases, some of these bands become more persistent. At the final stage, the last slip events occur at the same location. In particular, the ultimate failure plane is activated many times, akin to stick–slip phenomena.

A series of 57 digital images were acquired using a digital camera such that the physical size of one pixel is 4.3 μm. DIC is a technique that allows one to measure the displacement field between consecutive images of a mechanical test by looking for the best match between these images after a correction by this displacement field [14]. To the best of our knowledge, no such technique has ever been used in the context of BMGs.

Figure 2 shows incremental strain maps (i.e. consecutive images), where the strain refers to the component $\varepsilon_{zz}$ along the compression axis, $z$. DIC reaches subpixel resolution from the integration of the displacement over a zone that has a finite extent. In the present case, we used a code such that the displacement is decomposed over square bilinear finite-element shape functions [15] whose size is $35 \times 35$ μm$^2$ for which typical displacement uncertainties are of the order of 0.5 μm. It is observed that the strains are concentrated into very thin (one finite-element wide, or 35 μm) structures that are the trace of a kinematic discontinuity. A refined analysis leads to the conclusion that the support of the discontinuity is of the order of 5–10 μm (1–2 pixels) at most. The actual size may be much smaller, but it cannot be resolved with the present technique. The apparent vertical amplitude of the displace-

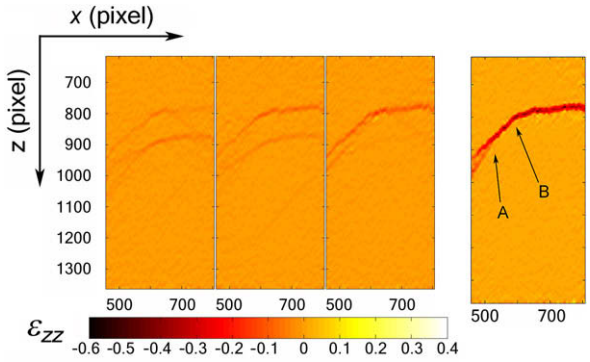


**Figure 2.** (Left) Three consecutive incremental strain maps obtained from DIC showing multiple slip systems being simultaneously active. (Right) Strain map prior to failure where A shows a branching point and B shows a kink produced by the intersection of two slip bands. The colour bar indicates the apparent strain level computed over 35 μm wide elements.

ment discontinuity is of the order of 5–10 μm, depending on the studied band. The geometry of the bands is much more accurately determined than that obtained from the temperature maps because of heat diffusion. The above reported observations concerning the overall variability and persistence of the different shear bands are confirmed through this analysis, with a much better accuracy. The final slip system, for example, that appears as a smooth elliptical shape from temperature maps, is here observed to be much rougher, with kink and branching as shown in Figure 2. This roughness is not an artefact of the DIC analysis, as will be shown below.

The most salient feature of this analysis is that it reveals a much more complex slip system than could have been guessed from the temperature maps. Bifurcations of shear bands, multiple slip systems, are clearly observed. It should be noted that, in contrast with IR pictures, the time interval (2 s) between consecutive images is such that several (2–5) slip events may develop. The cumulative effect of these mechanisms is observed, and one cannot separate them into individual events.

The multiplicity of different and parallel shear bands has already been mentioned several times in the literature [16–18], but only from post-mortem surface observations without any information on the time sequence of these bands. SEM images of the sample after failure show on the sample side the traces of shear bands. A large number of quasi-parallel shear bands support the previous observation of scatter of the shear band location. Moreover, if the dominant geometry of these surfaces is roughly planar and forming an angle of ca. 45° with respect to the compression axis (maximum shear stress), other traces correspond to a significantly different angle. It can also be seen that the sample is finally broken mostly through slip along surfaces that correspond to such shear bands, but these surfaces are connected by a step that is essentially a mode I crack, as can be seen in Figure 3. From these low-magnification SEM images, it is concluded that the failure surface (besides the above mentioned step) is not a perfect plane, but rather a rough surface.

The specimen side displays very irregular patterns of discontinuities with multiple crossings of very rough traces of slip surfaces. One can also see side branching, again confirming that the different slip events are not as simple as a planar slip system or a mode II or III crack. This observation also provides a plausible explanation for the formation of such a significant roughness, namely, the multiplicity of different weak surfaces created by past discontinuities promotes the partial mobilization of different slip systems that may not be completely kinematically compatible. This will further induce localization on side branches, micro-crack openings and contacting asperities.

The observation of the surface after fracture is also quite enlightening. On most of the surface (Fig. 4) characteristic "river" patterns appear, as often reported in the literature. They correspond to the separation of the two surfaces along an interface where the material has been brought up to the glass transition temperature, where viscous flow could take place. At very small scales, the surface smoothness is due to surface tension driven flow, which requires a very low viscosity because of the very short duration of slip. The origin of these lines is due to cavity (or bubble) nucleation and growth, which drag the viscous phase at the junction between neighbouring porosities. The presence of isotropic patterns indicates that the fracture was produced under mostly normal separation of the surfaces. However, the "river" pattern is often seen to be markedly anisotropic. This corresponds to a separation involving both normal and tangential displacement discontinuities (mixed mode cracks in the language of fracture mechanics). In Figure 4 a more surprising feature is observed, namely some parts of the surface show different slip directions forming a large angle (presumably in different episodes) in different zones of the final failure surface. Moreover, in addition to such river patterns, more brittle-like areas develop, which show micro-cracking.

These observations suggest a mechanism for the arrest of a slip event, and hence the fact that the material may withstand a number of these micro-instabilities without failure. The surface roughness along the discontinuity cannot allow for a pure tangential discontinuity. Hence some parts of the surface will tend to separate while others will slip with increasing normal pressure. While the former will lead to void nucleation (or damage), the latter is responsible for a hardening behaviour. Damage helps explain the final part of the load–displacement curve, where the stress level at which the last events are initiated drops significantly compared to the plateau regime. However, for the larger part of the plastic plateau, no apparent decrease in the flow stress is observed. This may be due to two reasons: first, initially, the roughness-induced dilatant behaviour is weak; and

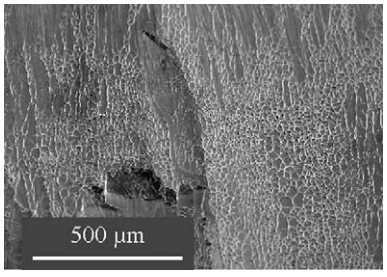


**Figure 3.** Failure surface showing both brittle micro-cracks (top and lower part of the picture) and river patterns characteristic of the separation of the surfaces along a region where viscous flow took place.

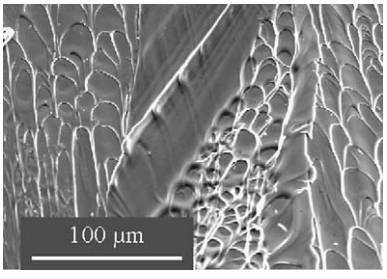


**Figure 4.** SEM observation of the specimen-free surface after failure. Different slip directions can be distinguished over the final failure surface.

second, because of large heat dissipation, melting of the material in the sheared region will allow for a good healing of the material after slip. If, however, cavitation is initiated, then surface tension will allow for the relaxation of stress concentration factors.

The reported observations, which come from the unique combination of fast IR images, DIC of photographic images and SEM scans, show that the shear failure of BMGs is more complex than anticipated in terms of geometry and sequence of localized strain regions. The multiplicity of different slip surfaces being activated at different times and the roughness of these surfaces provide a possible mechanism for the arrest of slip, and hence the large apparent strain to failure that was observed for this material.

J.Z. acknowledges the Ecole Normale Supérieure de Cachan for the International Scholarship Programme 2007–2008 and the National Basic Research Program of China (973 Program, No. 2007CB613900).

[1] W. Klement, R.H. Willens, P. Duwez, Nature 187 (1960) 869.
[2] A. Inoue, T. Zhang, T. Masumoto, Mater. Trans. 31 (1990) 425.
[3] H.S. Chen, Scripta Metall. 7 (1973) 931.
[4] W.J. Wright, R. Saha, W.D. Nix, Mater. Trans. 42 (2001) 642.
[5] A.C. Schuh, T.C. Hufnagel, U. Ramamurty, Acta Mater. 55 (2007) 4067.
[6] S.X. Song, H. Bei, J. Wadsworth, T.G. Nieh, Intermetallics 16 (2008) 813.
[7] J.J. Lewandowski, A.L. Greer, Nat. Mater. 5 (2006) 15.
[8] B. Yang, P.K. Liaw, G. Wang, M. Morrison, C.T. Liu, R.A. Buchanan, Y. Yokoyama, Intermetallics 12 (2004) 1265.
[9] B. Yang, M.L. Morrison, P.K. Liaw, R.A. Buchanan, G.Y. Wang, C.T. Liu, M. Denda, Appl. Phys. Lett. 86 (2005) 141904.
[10] B. Yang, P.K. Liaw, M. Morrison, C.T. Liu, R.A. Buchanan, J.Y. Huang, R.C. Kuo, J.G. Huang, D.E. Fielden, Intermetallics 13 (2005) 419.
[11] W.H. Jiang, H.H. Liao, F.X. Liu, H. Choo, P.K. Liaw, Metal. Mater. Trans. A 39 (2008) 1822.
[12] W.H. Jiang, G.J. Fan, F.X. Liu, G.Y. Wang, H. Choo, P.K. Liaw, Int. J. Plast. 24 (2008) 1.
[13] Y.H. Liu, G. Wang, R.J. Wang, D.Q. Zhao, M.X. Pan, W.H. Wang, Science 315 (2007) 1385.
[14] T.C. Chu, W.F. Ranson, M.A. Sutton, W.H. Peters, Exp. Mech. 25 (1985) 232.
[15] G. Besnard, F. Hild, S. Roux, Exp. Mech. 46 (2006) 789.
[16] J. Schroers, W.L. Johnson, Phys. Rev. Lett. 93 (2004) 255506.
[17] L. Liu, S.J. Pang, C.L. Ma, T. Zhang, Mater. Trans. 46 (2005) 2945.
[18] T. Zhang, F.J. Liu, S.J. Pang, R. Li, Mater. Trans. 48 (2007) 1157.